ACS Catalysis

Research Article

pubs.acs.org/acscatalysis

Kinetic Evidence for Bimolecular Nucleation in Supported-Transition-Metal-Nanoparticle Catalyst Formation in Contact with Solution: The Prototype Ir(1,5-COD)Cl/γ-Al_2O_3 to Ir(0)$_{\sim 900}$/γ-Al_2O_3 System

Joseph E. Mondloch and Richard G. Finke*

Department of Chemistry, Colorado State University, Fort Collins, Colorado 80523, United States

Supporting Information

ABSTRACT: Kinetic and mechanistic studies of the formation of supported-nanoparticle catalysts in contact with solution hold promise of driving the next generation syntheses of size, shape, and compositionally controlled catalysts. Recently, we studied the kinetics and mechanism of formation of a prototype Ir(0)$_{\sim 900}$/γ-Al_2O_3 supported-nanoparticle catalyst from Ir(1,5-COD)Cl/γ-Al_2O_3 in contact with solution (Mondloch, J.E.; Finke, R.G. *J. Am. Chem. Soc.* **2011**, *133*, 7744). Key kinetic evidence was extracted from γ-Al_2O_3- and acetone-dependent kinetic curves in the form of rate constants for nucleation (A → B, rate constant k_{1obs}) and autocatalytic surface growth (A + B → 2B, rate constant k_{2obs}), where A is nominally the Ir(1,5-COD)Cl/γ-Al_2O_3 and B the growing, supported Ir(0)$_n$/γ-Al_2O_3 nanoparticle. The resultant data provided evidence for a mechanism consisting of four main steps: Ir(1,5-COD)Cl(solvent) dissociation from the γ-Al_2O_3 support, then Ir(1,5-COD)Cl(solvent) solution-based nucleation, fast nanoparticle capture by the γ-Al_2O_3 and then subsequent nanoparticle growth between Ir(0)$_n$/γ-Al_2O_3 and Ir(1,5-COD)Cl(solvent) in solution. While the k_{2obs} vs [γ-Al_2O_3]$_{sus}$ and [acetone] autocatalytic surface growth rate constants were nicely accounted for by the proposed mechanism, the k_{1obs} nucleation rate constants were only "roughly" accounted for by the previously proposed *unimolecular* solution-based nucleation mechanism. Hence, in the present work we have reexamined that γ-Al_2O_3- and acetone-dependent nucleation data in light of the hypothesis that nucleation is actually *bimolecular*. Extracting bimolecular, $k_{1obs(bimol)}$, rate constants by curve-fitting yields qualitative (i.e., visual inspection) as well as quantitative (i.e., increased R^2 values) *evidence consistent with and strongly supportive of solution-based bimolecular nucleation* (A + A → 2B, rate constant $k_{1obs(bimol)}$) for the Ir(1,5-COD)Cl/γ-Al_2O_3 to Ir(0)$_{\sim 900}$/γ-Al_2O_3 system in contact with acetone. The extracted $k_{1obs(bimol)}$ vs [γ-Al_2O_3]$_{sus}$ and [acetone] data in turn rule out the solution-based unimolecular mechanism (as well as a hypothetical termolecular nucleation mechanism). This study is significant in that (i) it is the first evidence for bimolecular nucleation in transition-metal nanoparticle formation in any system, be it ligand- or support-stabilized nanoparticle formation in solution or on solid-supports in gas−solid systems, and since (ii) it shows that mechanism-based nanoparticle size control, previously demonstrated to depend on k_{1obs}, is hereby shown to actually depend on $2k_{1obs(bimol)}$[A]^1. Furthermore, the results presented are of broad significance since (iii) they are part of a growing literature suggesting that simple, bimolecular nucleation may well be closer to the rule, rather than the exception, in a range of systems across nature, and since the results herein (iv) disprove, for at least the present system, the higher nuclearity nucleation kinetics suggested by nucleation theory and its often discussed critical nucleus concept. The results also (v) argue for the new concept of a "kinetically effective nucleus", in this case binuclear M_2 (M = metal).

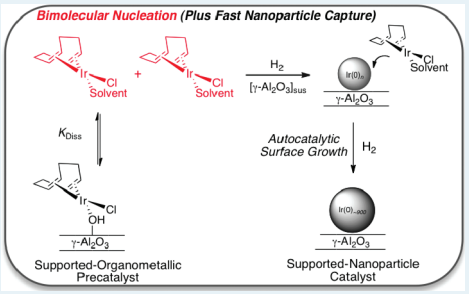

KEYWORDS: *bimolecular nucleation, mechanism of nanoparticle formation, heterogeneous catalyst synthesis in contact with solution*

INTRODUCTION

Establishing the mechanisms of formation of supported-nanoparticle heterogeneous catalysts is essential to developing routine synthetic routes capable of producing the desired size, shape and compositionally controlled heterogeneous catalysts.[1] This is important as the nanoparticle size, shape, and composition dictate key catalytic properties including activity, selectivity, and lifetime.[2] A recent review of the literature,[3] of the kinetics and mechanisms of supported-nanoparticle formation, revealed that systems *in contact with solution* (i.e., with a *liquid* in contact with the solid oxide) are an emerging, potentially better way to synthesize supported-nanoparticle heterogeneous catalysts. Such liquid−solid systems can also be studied kinetically and mechanistically en route to rational improvements in those syntheses.

In a recent series of papers[4,5] the prototype Ir(1,5-COD)Cl/γ-Al_2O_3 precatalyst system *in contact with solution* was employed to synthesize the resultant, high catalytic activity and good lifetime Ir(0)$_{\sim 900}$/γ-Al_2O_3 supported-nanoparticle catalyst (8,200 turnovers/h and 220,000 total turnovers for the

Received: December 8, 2011
Revised: January 8, 2012
Published: January 25, 2012

hydrogenation of cyclohexene[4]). The criteria that define a prototype system are repeated in a footnote for the interested reader.[6] The Ir(1,5-COD)Cl/γ-Al_2O_3 precatalyst and resulting Ir(0)$_{\sim 900}$/γ-Al_2O_3 supported-nanoparticle catalyst were fully characterized by a range of methods (Scheme 1) including

Scheme 1. Recently Developed[4] Ir(1,5-COD)Cl/γ-Al_2O_3 (Left) to Ir(0)$_{\sim 900}$/γ-Al_2O_3[a] Supported-Nanoparticle Heterogeneous Catalyst Formation System Synthesized in Contact with Solution

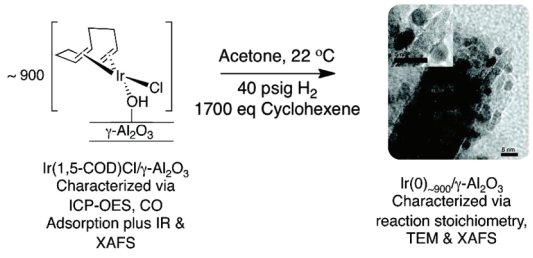

[a]Right, TEM imaging with scale bars of 5 nm.

inductively coupled plasma optical emission spectroscopy, CO/IR spectroscopy trapping experiments, X-ray absorbance fine structure (XAFS) spectroscopy, transmission electron microscopy (TEM), and the balanced stoichiometry for the supported-nanoparticle formation reaction.[4] The system in Scheme 1 is, at present, the most thoroughly studied (at least kinetically and mechanistically) supported-nanoparticle formation system in contact with solution.[3]

Key mechanistic results of that recent work[4,5] include (i) that the kinetic curves are sigmoidal and well-fit to a two-step mechanism[7] consisting of nucleation (A → B, rate constant k_{1obs}) followed by autocatalytic surface growth (A + B → 2B, rate constant k_{2obs});[4] and (ii) that the more detailed mechanism consists of the four main steps of a K_{Diss} equilibrium between Ir(1,5-COD)Cl/γ-Al_2O_3 ($[Ir^I/Al_2O_3]_{sus}$) and Ir(1,5-COD)Cl(solvent) (Ir^I*solvent), Ir(1,5-COD)Cl(solvent) solution-based nucleation (k_1'), fast nanoparticle capture by γ-Al_2O_3 ($[Al_2O_3]_{sus}$), and subsequent solid-oxide-based supported-nanoparticle growth between Ir(0)$_n$/γ-Al_2O_3 ($[Ir(0)/Al_2O_3]_{sus}$) and Ir(1,5-COD)Cl(solvent) in solution, all as shown in Scheme 2 (in bold).[5]

Kinetic data consistent with the mechanism in bold in Scheme 2 were obtained in the form of k_{1obs} and k_{2obs} dependencies on the $[\gamma\text{-}Al_2O_3]_{sus}$ and [acetone] "concentrations", vide infra; the $[\gamma\text{-}Al_2O_3]_{sus}$ and [acetone] dependencies also disproved the "all solution" (right most pathway) and "all solid-oxide-based" (left most) nucleation and growth pathways.[5] Importantly, the values of the curve-fit-determined K_{Diss} and K_{Diss}' equilibrium constants *were independently verified* via gas−liquid chromatography (GLC) and UV−vis spectroscopy, respectively.[5] While the k_{2obs} vs $[\gamma\text{-}Al_2O_3]_{sus}$- and [acetone]-dependent kinetic data are nicely and quantitatively accounted for by the proposed mechanism, the k_{1obs} data were only roughly accounted for by the proposed mechanism and merits further investigation, as detailed next.

Previously Obtained Ir(1,5-COD)Cl/γ-Al_2O_3 to Ir(0)$_{\sim 900}$/γ-Al_2O_3 Nucleation k_{1obs} vs $[\gamma\text{-}Al_2O_3]_{sus}$ and [Acetone] Dependencies. Shown in Figure 1 are the dependencies of the k_{1obs} rate constants on the γ-Al_2O_3 (top) and acetone (bottom) concentrations. The k_{1obs} rate constants have a range of ~10^1 over the $[\gamma\text{-}Al_2O_3]_{sus}$ and [acetone] concentrations

Scheme 2. Recently Proposed[5] Supported-Nanoparticle Heterogeneous Catalyst Formation Mechanism (in Bold) for the Ir(0)$_{\sim 900}$/γ-Al_2O_3 Supported-Nanoparticle Formation System in Contact With Solution[a]

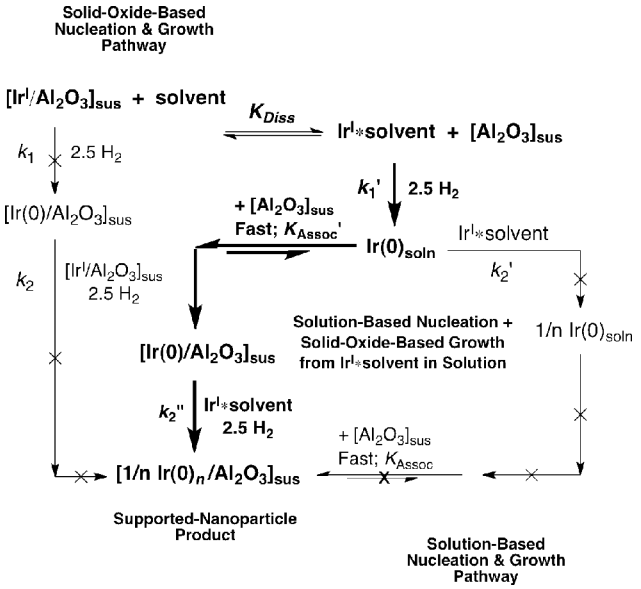

[a]In the scheme, Ir(1,5-COD)Cl/γ-Al_2O_3, Ir(1,5-COD)Cl(solvent), and γ-Al_2O_3 are abbreviated as $[Ir^I/Al_2O_3]_{sus}$, Ir^I*solvent and $[Al_2O_3]_{sus}$, respectively.

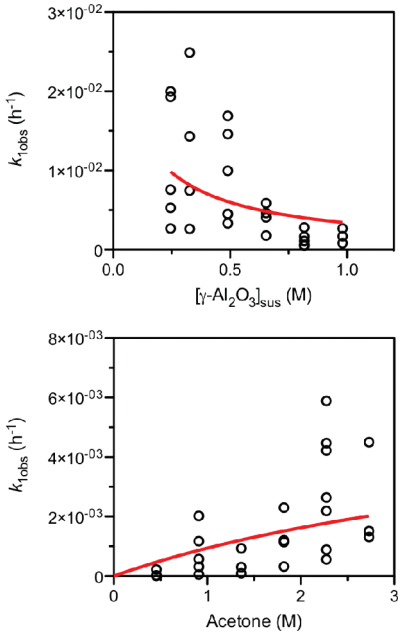

Figure 1. Top, the previously reported[5] dependence of k_{1obs} on $[\gamma\text{-}Al_2O_3]_{sus}$ (circles). The red line is the nonlinear least-squares fit to the unimolecular-based eq 1 while constraining $K_{Diss} = 1.3 \times 10^{-2}$ as defined in the pathway in bold in Scheme 2, vide supra. Bottom, the previously reported dependence of k_{1obs} on [acetone] (circles). The red line is the nonlinear least-squares fit to eq 2 while constraining $K_{Diss}' = 3 \times 10^{-2}$. Note the failure of the fits in both the top and bottom to curve upward at lower (top) and higher (bottom) concentrations so as to optimally account for the data.

studied, and the curve-fits (red lines) in Figure 1 are to the previously derived[5] k_{1obs} equations, reproduced as eqs 1 and 2 herein. While the scatter in the k_{1obs} vs $[\gamma\text{-}Al_2O_3]_{sus}$ and

dx.doi.org/10.1021/cs2006422 | ACS Catal. 2012, 2, 298−305

[acetone] data may at first glance be bothersome, the nucleation data are actually some of the most extensive and precise data presently available for such a system. Also relevant here is that nucleation rate constants are known to have a scatter of $\sim 10^{1.2}$ in even the best-studied nanoparticle formation systems to date[8] and can have a range of up to $\sim 10^{8}$ in other systems.[9] Measuring nucleation rate constants at even the level of scatter shown in Figure 1 is neither routine nor trivial.

$$k_{1\mathrm{obs}} = \frac{k_1' K_{\mathrm{Diss}}[\mathrm{solvent}]_t}{[\mathrm{Al_2O_3}]_{\mathrm{sus},t} + K_{\mathrm{Diss}}[\mathrm{solvent}]_t} \quad (1)$$

$$k_{1\mathrm{obs}} = \frac{k_1'' K_{\mathrm{Diss}}'[\mathrm{solvent}]_t}{[\mathrm{Al_2O_3}]_{\mathrm{sus},t} + K_{\mathrm{Diss}}[\mathrm{solvent}]_t} \quad (2)$$

While the fits to eqs 1 and 2 do, as previously noted, "qualitatively account for the rough shape of the curves" in Figure 1,[10] the fits shown resulted only if the K_{Diss} and K_{Diss}' equilibriums were constrained to their known values of 1.3×10^{-2} and 3.0×10^{-2}, respectively. In other words, nonlinear least-squares fits to eqs 1 and 2 did not converge when *both* K_{Diss} and k_1' (Figure 1) or K_{Diss}' and k_1''[10] were allowed to vary. In addition, visually it seems as if the resultant curves in Figure 1 do not fully account for the full $k_{1\mathrm{obs}}$ vs $[\gamma\text{-}\mathrm{Al_2O_3}]_{\mathrm{sus}}$ and [acetone] data sets (e.g., the highest values of $[\gamma\text{-}\mathrm{Al_2O_3}]_{\mathrm{sus}}$). A deeper look at the nucleation kinetics seemed in order, and is the focus of the present contribution.

On reflection we reasoned that a *bimolecular nucleation* mechanism both makes physical sense (i.e., the combination of at least 2 species en route to higher nuclearity nanoparticles) and might very well provide better fits to the $[\gamma\text{-}\mathrm{Al_2O_3}]_{\mathrm{sus}}$ and [acetone] data, that is, A + A → 2B (vide infra). One reason this occurred to us is that higher-order nucleation, and therefore fits to the unimolecular (i.e., A → B, rate constant $k_{1\mathrm{obs}}$) nucleation mechanism, can be kinetically hidden since [A] is effectively constant (i.e., $[\mathrm{A}] \cong [\mathrm{A}]_0$) during the induction period of the sigmoidal kinetic curves. This means that a true bimolecular nucleation with $k_{1\mathrm{true}}[\mathrm{A}]^2$ can masquerade as the pseudo-first-order $k_{1\mathrm{obs}}[\mathrm{A}] = (k_{1\mathrm{true}}[\mathrm{A}])[\mathrm{A}]$.

In addition, for some time we have had preliminary evidence for bimolecular nucleation in solution nanoparticle formation from our well-studied, $(1,5\text{-COD})\mathrm{Ir}^{\mathrm{I}}\cdot\mathrm{P_2W_{15}Nb_3O_{62}}^{8-}$, polyoxoanion-stabilized nanoparticle formation system, work that is nearing completion.[11] Finally, some evidence exists for the formation of dimeric complexes en route to higher nuclearity metal species, specifically extended X-ray absorbance fine structure and infrared spectroscopic structural evidence for the formation of a dimeric "$\mathrm{Ir_2(CO)_8}$" species en route to $\mathrm{Ir_4(CO)_{12}}$ (in a gas−solid system) has been reported by Gates' group.[12] Also relevant here is computational evidence suggesting the formation of Pt−Pt dimers,[13] structural evidence consistent with the formation of $\mathrm{Ag_2}^{+}$,[14] $\mathrm{Pt_2(CH_3)_8(AlCH_3)_2}$[15] and $\mathrm{Au_2Cl_6}^{2-}$ dimers[16]—albeit without the necessary kinetic evidence to support or refute that these dimeric species are kinetically competent intermediates on path to the ligand-stabilized $\mathrm{M(0)}_n$ nanoparticle products. A general review of what is known about ligand-stabilized nanoparticle formation in solution is also available.[17] In short, literature hints are available suggesting that bimolecular nucleation deserves closer scrutiny.

However, despite the above-noted studies, to date *no kinetic evidence has previously appeared supporting bimolecular nucleation in transition-metal nanoparticle formation.* Moreover, there is no prior report or even mention of bimolecular nucleation in the limited literature of supported-nanoparticle heterogeneous catalyst formation reactions in contact with solution.[3]

Herein we (i) test the proposed binuclear nucleation hypothesis, A + A → 2B, by analyzing the existing $[\gamma\text{-}\mathrm{Al_2O_3}]_{\mathrm{sus}}$- and [acetone]-dependent nucleation data and extracting $k_{1\mathrm{obs(bimol)}}$ rate constants. Both qualitative, visual inspection and quantitative curve-fitting (R^2 value) statistics provide compelling evidence for *bimolecular*, solution-based nucleation from 2 equiv of Ir(1,5-COD)Cl(solvent) that has dissociated off the Ir(1,5-COD)Cl/γ-$\mathrm{Al_2O_3}$ precatalyst, that is, where the true [A] is given by [Ir(1,5-COD)Cl(solvent)] = constant × [Ir(1,5-COD)Cl/γ-$\mathrm{Al_2O_3}$] (constant = $K_{\mathrm{Diss}}/[\mathrm{solvent}]_t[\gamma\text{-}\mathrm{Al_2O_3}]_{\mathrm{sus},t}$). The results are of broader significance in that (ii) they are consistent with a growing literature suggesting bimolecular nucleation phenomena may well be more general in multiple systems across nature (e.g., in systems ranging from protein aggregation to aerosol formation, vide infra), and therefore that (iii) classical nucleation theory, and its critical nucleus concept of a higher molecularity nucleus, M_n, are *not supported* in cases where nucleation is demonstrated kinetically to be bimolecular. It is hard to overstate the importance of such evidence against classical nucleation theory, that theory having dominated, and in a number of ways misled,[18] discussions of nucleation and growth across nature since the time of LaMer's classic—but problematic—1950 paper.[19]

EXPERIMENTAL SECTION

Monitoring the $\mathrm{Ir(0)}_{\sim 900}/\gamma\text{-}\mathrm{Al_2O_3}$ Supported-Nanoparticle Formation Kinetics and Extraction of the $k_{1\mathrm{obs(bimol)}}$ Rate Constants. The key experimental details are identical to those previously published.[5] Briefly, the $\mathrm{Ir(0)}_{\sim 900}/\gamma\text{-}\mathrm{Al_2O_3}$ supported-nanoparticle formation kinetics (with varying $[\gamma\text{-}\mathrm{Al_2O_3}]_{\mathrm{sus}}$ and [acetone]) were followed in contact with solution using the now well-precedented cyclohexene reporter reaction method,[4,5,7,20] Scheme 3, in which B is the growing $\mathrm{Ir(0)}_n/\gamma\text{-}\mathrm{Al_2O_3}$ nanoparticle surface. The cyclohexene reporter reaction reports on and amplifies the amount of nanoparticle catalyst, B, present,[7] Scheme 3.

Scheme 3. Cyclohexene Reporter Reaction Method Used to Follow the $\mathrm{Ir(0)}_{\sim 900}/\gamma\text{-}\mathrm{Al_2O_3}$ Supported-Nanoparticle Formation Kinetics

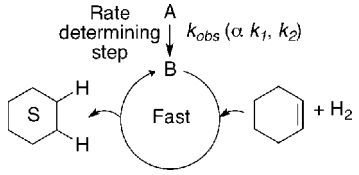

Experimentally the $\mathrm{Ir(0)}_{\sim 900}/\gamma\text{-}\mathrm{Al_2O_3}$ supported-nanoparticle formation kinetics were followed by monitoring the H_2 reduction of Ir(1,5-COD)Cl/γ-$\mathrm{Al_2O_3}$ in a previously described apparatus,[7,9,21] which continuously monitors H_2 pressure loss. The H_2 uptake curves were then converted into cyclohexene (M) curves using the previously established 1:1 H_2/cyclohexene stoichiometry.[7,22]

Data Handling. The $k_{1\mathrm{obs(bimol,curvefit)}}$ rate constants were extracted from the previously collected[5] $[\gamma\text{-}\mathrm{Al_2O_3}]_{\mathrm{sus}}$- and [acetone]-dependent kinetic data using nonlinear least-squares fitting in GraphPad Prism 5. Specifically, the sigmoidal cyclohexene loss kinetic curves were fit to eq 3 (derived in

dx.doi.org/10.1021/cs2006422 | ACS Catal. 2012, 2, 298−305

the Supporting Information), which is the integrated rate equation of the *phenomenological* two-step mechanism consisting of *bimolecular nucleation* (A + A → 2B, rate constant $k_{1obs(bimol,curvefit)}$) followed by autocatalytic surface growth (A + B → 2B, rate constant $k_{2obs(curvefit)}$). To account for the stoichiometry of the pseudoelementary step,[7] the $k_{1obs(bimol,curvefit)}$ values were corrected for by a factor of 1700/2 = 850 as detailed in the Supporting Information, a correction factor that yielded the $k_{1obs(bimol)}$ rate constants (i.e., 1700 × $k_{1obs(bimol,curvefit)}$ = 2 × $k_{1obs(bimol)}$).

$$[A]_t = \left\{k_{2obs(curvefit)}[A]_0\right\} \Big/ \left\{2k_{1obs(bimol,curvefit)}(\exp^{k_{2obs(curvefit)}[A]_0 t} - 1) + k_{2obs(curvefit)}\right\} \quad (3)$$

The $k_{1obs(bimol)}$ vs $[\gamma\text{-}Al_2O_3]_{sus}$ and [acetone] curves were then plotted and fit using weighted nonlinear least-squares analysis in GraphPad Prism 5 (i.e., fit with eqs 9 and 10 respectively, vide infra). Relative weighting (i.e., $1/Y^2$) was used as the average absolute distance, between the curve and the data points, is larger when Y is larger. Use of $1/Y^2$ weighted nonlinear least-squares analysis minimizes the sum-of-squares of eq 4.[23] For the $[\gamma\text{-}Al_2O_3]_{sus}$ dependent $k_{1obs(bimol)}$ curve-fitting, [acetone] was taken to be constant at a value of 11.37 M. For the [acetone] dependent fitting, $[\gamma\text{-}Al_2O_3]_{sus}$ was taken to be constant at a value of 0.163 M.

$$\sum \frac{1}{Y^2}(Y_{Data} - Y_{Curve})^2 \quad (4)$$

RESULTS AND DISCUSSION

Proposed Mechanism: Bimolecular Ir(1,5-COD)Cl-(solvent) Solution-Based Nucleation. The proposed mechanism, Scheme 4, is identical to that shown back in

Scheme 4. Proposed Bimolecular Ir(1,5-COD)Cl(solvent) Solution-Based Nucleation Mechanism for the Ir(1,5-COD)Cl/γ-Al_2O_3 to Ir(0)$_{\sim 900}$/γ-Al_2O_3 Supported-Nanoparticle Formation Reaction in Contact with Solution[a]

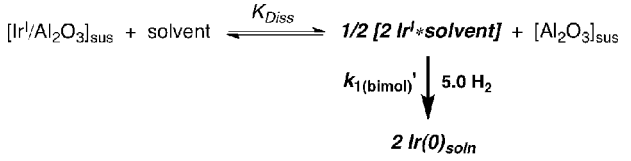

[a]The use of the notation "1/2[2Ir^I·solvent]" in the above scheme is just a way to both (a) show a balanced dissociative equilibrium with the same definition of K_{Diss} as used before,[4] while also (b) indicating the bimolecular nucleation step of 2 Ir^I·solvent →2Ir(0)$_{soln}$.

Scheme 2, *except* Scheme 4 *now contains a bimolecular Ir(1,5-COD)Cl(solvent) solution-based nucleation step*. Combined with our previous work,[5] the proposed mechanism consists of a dissociative equilibrium between Ir(1,5-COD)Cl/γ-Al_2O_3 and Ir(1,5-COD)Cl(solvent). Bimolecular nucleation then is proposed to occur from the dissociated "homogeneous" Ir(1,5-COD)Cl(solvent) complex in solution, followed by a fast nanoparticle capture step by the γ-Al_2O_3. Subsequently, "heterogeneous" solid-oxide-based nanoparticle growth is known to occur between Ir(0)$_n$/γ-Al_2O_3 and the dissociated Ir(1,5-COD)Cl(solvent) complex.[5]

As was previously justified,[5,24] in the kinetic expressions derived next (the full derivations of which are given in the Supporting Information), the Ir(1,5-COD)Cl/γ-Al_2O_3 precatalyst and γ-Al_2O_3 have necessarily been approximated as being "homogeneously suspended in solution". Here, we focus on the nucleation step only as the nanoparticle growth step is identical to that previously derived.[5] We start from the rate equation for the bimolecular nucleation step (i.e., A + A → 2B), eq 5.

$$-\frac{d[Ir^I/Al_2O_3]_{sus}}{dt} = 2k_{1(bimol)}'[Ir^I{*}solvent]_t^2 \quad (5)$$

In eq 5 and the equations that follow, the subscript "t" denotes each species as a function of time, while the subscript "i" represents initial concentrations. Next, eq 5 is expressed in terms of the $[Ir^I/Al_2O_3]_{sus,i}$ that we experimentally begin with. Solving eq 6 for $[Ir^I/Al_2O_3]_{sus,t}$, followed by substitution into the mass balance equation are necessary steps in the complete derivation.

$$K_{Diss} = \frac{[Ir^I{*}solvent]_t[Al_2O_3]_{sus,t}}{[Ir^I/Al_2O_3]_{sus,t}[solvent]_t} \quad (6)$$

$$[Ir^I/Al_2O_3]_{sus,i} = [Ir^I/Al_2O_3]_{sus,t} + [Ir^I{*}solvent]_t \quad (7)$$

Substitution of the resultant $[Ir^I{*}solvent]_t$ equation back into eq 5 yields the relevant rate equation for Scheme 4, eq 8, where $k_{1obs(bimol)}$ is defined by (see the Supporting Information for details of the derivation, eq 9 is equivalent to S13 in the Supporting Information) by eq 9.

$$-\frac{d[Ir^I/Al_2O_3]_{sus}}{dt} = k_{1obs(bimol)}[Ir^I/Al_2O_3]_{sus,i}^2 \quad (8)$$

$$k_{1obs(bimol)} = \left\{2k_{1(bimol)}'K_{Diss}^2[solvent]_t^2\right\} \Big/ \left\{[Al_2O_3]_{sus,t}^2 + 2[Al_2O_3]_{sus,t}[solvent]_t + K_{Diss}^2[solvent]_t^2\right\} \quad (9)$$

Equation 9, predicts, as before,[5] that $k_{1obs(bimol)}$ will decrease with increasing $[\gamma\text{-}Al_2O_3]_{sus}$ and increase with increasing [solvent], but now with a higher-order, quadratic dependence that includes squared terms in $[\gamma\text{-}Al_2O_3]^2_{sus,t}$ and $[solvent]_t^2$.

Analysis of the $k_{1obs(bimol)}$ vs $[\gamma\text{-}Al_2O_3]_{sus}$-Dependent Kinetic Data to the Solution-Based Bimolecular Nucleation Mechanism. The $k_{1obs(bimol)}$ rate constants were extracted from the previously obtained $[\gamma\text{-}Al_2O_3]_{sus}$-dependent kinetic data[5] via nonlinear least-squares fitting to eq 3. An example fit is shown in Figure 2; the fits to the data by eq 3 are in general excellent (R^2 = 0.999). As a check on the $[\gamma\text{-}Al_2O_3]_{sus}$-dependent bimolecular data treatment, our analysis requires that the relationship $2k_{1obs(bimol)}[A]^2 = k_{1obs}[A]$ be satisfied. Indeed, the values of $2k_{1obs(bimol)}[A]^2$ and $k_{1obs}[A]$ from the $k_{1obs(bimol)}$ and k_{1obs} rate constants shown in Figures 3 and 1 agree within an expected experimental range of 1.1 to 1.5 (i.e., $2k_{1obs(bimol)}[A]^2/k_{1obs}[A]$ = 1.1 to 1.5).

The $k_{1obs(bimol)}$ rate constants are plotted vs $[\gamma\text{-}Al_2O_3]_{sus}$ in Figure 3; qualitatively $k_{1obs(bimol)}$ decreases with increasing $[\gamma\text{-}Al_2O_3]_{sus}$, consistent with the proposed bimolecular nucleation mechanism shown in Scheme 4 and eq 9. Significantly, the *unconstrained* fit of the bimolecular nucleation mechanism, eq 9 (i.e., the red line), to the $k_{1obs(bimol)}$ vs $[\gamma\text{-}Al_2O_3]_{sus}$ data is shown

dx.doi.org/10.1021/cs2006422 | ACS Catal. 2012, 2, 298–305

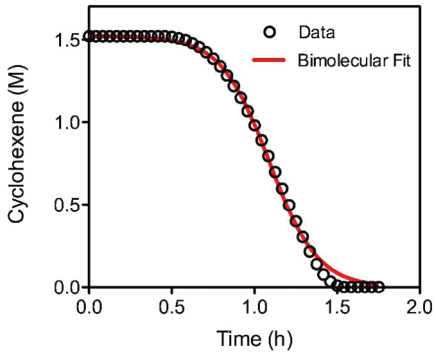

Figure 2. Representative example fit of [γ-Al_2O_3]-dependent supported-nanoparticle formation kinetic data (e.g., 0.49 M [γ-Al_2O_3]$_{sus}$) to the two-step bimolecular nucleation mechanism (i.e., eq 3). The small deviations at the end of the reaction are analogous to those seen before,[7] and are likely due to some particle-size dependence of the autocatalytic growth step.[19]

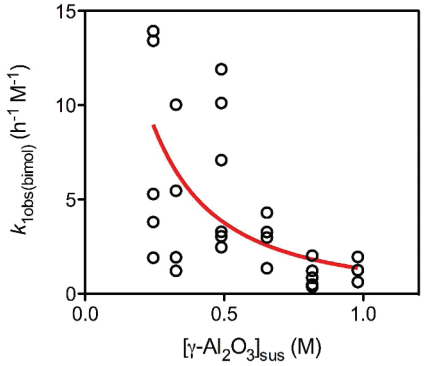

Figure 3. $k_{1obs(bimol)}$ vs [γ-Al_2O_3]$_{sus}$ data (circles) and fit (red line) to eq 9 derived from the Ir(1,5-COD)Cl(solvent)-based bimolecular nucleation mechanism (Scheme 4).

in Figure 3. Visually/qualitatively, the bimolecular nucleation mechanism (i.e., eq 9) more readily accounts for the full [γ-Al_2O_3]$_{sus}$-dependent nucleation data set—especially at higher [γ-Al_2O_3]$_{sus}$ concentrations and the upturn at lower [γ-Al_2O_3]$_{sus}$ concentrations—when compared to the unimolecular nucleation mechanism fit (i.e., eq 1) shown back in Figure 1.

Quantitatively,[25] the R^2 value is also superior if one compares R^2 values where K_{Diss} is constrained in both cases so that the R^2 values are rigorously comparable (0.421 for the bimolecular nucleation mechanism vs 0.309 for the unimolecular mechanism). The scatter in the nucleation kinetic data does result in a low R^2 value, but again recall that this is expected (i.e., recall the discussion of the errors of ~$10^{1.2}$ in even the most thoroughly kinetically studied solution nanoparticle formation system[8]). Overall, the bimolecular mechanism (Scheme 4, eq 9) fits the observed nucleation [γ-Al_2O_3]$_{sus}$-dependent data better by a factor of ~36%.

Arguably more significant is that eq 9 converges on the $k_{1obs(bimol)}$ vs [γ-Al_2O_3]$_{sus}$ data in an *unconstrained fit*, that is, when both K_{Diss} and $k_{1(bimol)}'$ are allowed to vary. The resultant fit-determined K_{Diss} and $k_{1(bimol)}'$ values are 2(1) × 10^{-2} and 20(16) h^{-1} M^{-1}, respectively. Pleasingly, given the inherent scatter in the data, the resultant unconstrained fit-determined K_{Diss} equilibrium value of 2(1) × 10^{-2} *is identical within experimental error to both of the previously reported* K_{Diss} *equilibrium values;* K_{Diss} = 1.3(6) × 10^{-2} *from fitting the* k_{2obs} *vs* [γ-Al_2O_3]$_{sus}$ *data, while the independently GLC-determined* K_{Diss} *equilibrium was found to be* 1.1(2) × 10^{-2}.[5] In short, the evidence for bimolecular nucleation is strong despite the unavoidable scatter in the data: (i) a fit that is now able to converge without constraining any variables; (ii) statistically superior fits result if both fits are constrained, and then there is also (iii) the resultant good agreement between the independently determined K_{Diss} equilibrium values.

Analysis of the $k_{1obs(bimol)}$ vs [Acetone]-Dependent Kinetic Data to the Solution-Based Bimolecular Nucleation Mechanism. The $k_{1obs(bimol)}$ rate constants were also extracted from the previously obtained [acetone]-dependent kinetic data[5] via nonlinear least-squares fitting to eq 3. An example fit is shown in Figure 4; again the fits to the data by eq

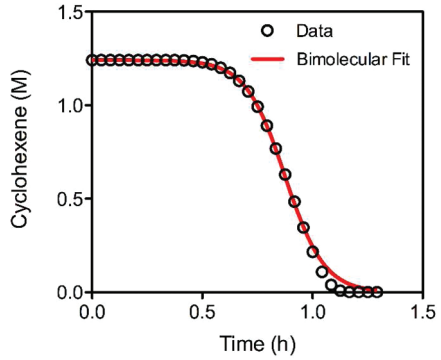

Figure 4. Representative example fits of [acetone]-dependent supported-nanoparticle formation kinetic data (e.g., 2.27 M [acetone]) to the two-step bimolecular nucleation mechanism (i.e., eq 3). Again, the small deviations at the end of the reaction are analogous to those seen before,[7] and are likely due to some particle-size dependence of the autocatalytic growth step.[19]

3 are excellent (R^2 = 0.999). As a check on the acetone-dependent bimolecular data treatment, our analysis again requires that the relationship $2k_{1obs(bimol)}[A]^2 = k_{1obs}[A]$ be satisfied. Once again, the acetone-dependent values of $2k_{1obs(bimol)}[A]^2$ and $k_{1obs}[A]$ from the $k_{1obs(bimol)}$ and k_{1obs} rate constants shown in Figures 5 and 1 agree within an expected experimental range of 1.0 to 1.8 (i.e., $2k_{1obs(bimol)}[A]^2/k_{1obs}[A]$ = 1.0 to 1.8).

The $k_{1obs(bimol)}$ rate constants are plotted vs [acetone] in Figure 5;[26] qualitatively $k_{1obs(bimol)}$ increases with increasing [acetone], again consistent with the proposed bimolecular nucleation mechanism shown in Scheme 4.

As before,[5,10] a slightly modified form of eq 9, eq 10 (derived in the Supporting Information), was needed to fit the [acetone]-dependent kinetic data collected under the mixed solvent conditions of cyclohexane plus acetone.

$$k_{1obs(bimol)} = \left\{2k_{1(bimol)}''K_{Diss}^{2}{}'[solvent]_t^2\right\} \Big/ \left\{[Al_2O_3]_{sus,t}^2 + 2[Al_2O_3]_{sus,t}[solvent]_t + K_{Diss}^{2}{}'[solvent]_t^2\right\} \quad (10)$$

The constrained fit of eq 10 (red line) to the $k_{1obs(bimol)}$ vs [acetone] data are shown in Figure 5. In contrast to the [γ-Al_2O_3]$_{sus}$-dependent nucleation data and the fit to eq 9, eq 10 could not converge on the [acetone]-dependent nucleation data without constraint of K_{Diss}' to its known value of 3.0 × 10^{-2}.[5] Despite this, visually eq 10 more readily accounts for the full range of the [acetone]-dependent nucleation data vs the

dx.doi.org/10.1021/cs2006422 | ACS Catal. 2012, 2, 298–305

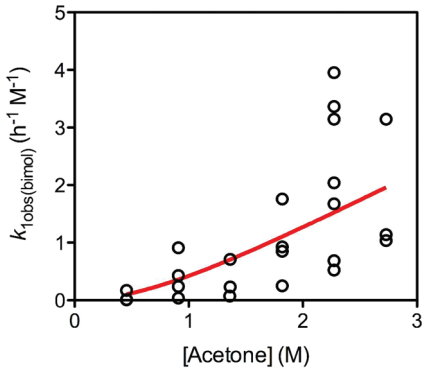

Figure 5. $k_{1obs(bimol)}$ vs [acetone] data (circles) and fit (red line) to eq 10 derived from the solution-based bimolecular nucleation mechanism (see the Supporting Information, Scheme S3).

unimolecular fit (i.e., eq 2) shown back in Figure 1. The resultant value for $k_{1(bimol)}''$ was found to be 9(1) h^{-1} M^{-1}. In addition, the R^2 value for the fit to the bimolecular mechanism is 0.424, while R^2 is only 0.248[26,27] for the fit to the unimolecular mechanism (comparing, in this case, constrained fits in both cases so that the comparison is rigorous). This is a statistically significant ~71% increase in R^2 for the bimolecular nucleation mechanism. In short, the [acetone]-dependent nucleation data are consistent with and supportive of the bimolecular nucleation mechanism shown in Scheme 4.

Disproof of a Hypothetical, Solution-Based, Termolecular Nucleation Mechanism. The bimolecular nucleation mechanism would be supported even further if a net termolecular mechanism, that is a mechanism[28] α $[A]^3$, could be ruled out—in part since doing so also would argue strongly against the even higher nucleation orders which tend to result from classical nucleation theory and its critical nucleus concept. Hence, this was done next.

The needed derivations for a net termolecular mechanism were done (Supporting Information, eqs S31 to S43), and attempted fits (Supporting Information, Figures S1 and S2) are provided in the Supporting Information for the interested reader. The key results, which provide good evidence *against* a net termolecular pathway and, therefore, provide additional support for the bimolecular pathway, are summarized next.

An unconstrained fit using Supporting Information, eq S40 derived for the hypothetical termolecular mechanism did converge on the $k_{1obs(bimol)}$ vs $[\gamma\text{-}Al_2O_3]_{sus}$ data (Supporting Information, Figure S1). *However*, the resultant K_{Diss} value is not in agreement with its independently measured value of $1.3(6) \times 10^{-2}$.[5] Attempts to constrain K_{Diss} to its known value of 1.3×10^{-2} resulted in inferior fits to the $k_{1obs(bimol)}$ vs $[\gamma\text{-}Al_2O_3]_{sus}$ data (i.e., and in comparison to the fits using the bimolecular nucleation mechanism). Specifically, (i) the termolecular mechanism could *not* account for the full range of $[\gamma\text{-}Al_2O_3]_{sus}$-dependent data (Supporting Information, Figure S2), and (ii) the fits are statistically worse than the bimolecular mechanism based on the R^2 values. In addition, attempts to fit the $k_{1obs(bimol)}$ vs [acetone] data to Supporting Information, eq S43, with or without constraint of the K_{Diss}' equilibrium, were unsuccessful. Finally, and as a control, to ensure the termolecular treatment of the $k_{1obs(bimol)}$ data did not affect any of the mechanistic conclusions, we fit the k_{1obs} vs $[\gamma\text{-}Al_2O_3]_{sus}$ and [acetone] data to the bimolecular mechanism (shown in the Supporting Information). As expected, the bimolecular mechanism more readily accounts for the k_{1obs} vs $[\gamma\text{-}Al_2O_3]_{sus}$ and [acetone] data (see Supporting Information, Figures S3 and S4). In short, the hypothetical termolecular mechanism is hereby disproven, a result which provides additional evidence consistent with and supportive of the bimolecular nucleation mechanism.

Finally, the reader who is interested in understanding the strengths and weaknesses of the 2-step, continuous (now bimolecular) nucleation, then autocatalytic growth mechanism[7] that underpins the present study is directed to a detailed discussion of those plus/minus points elsewhere—strengths/weaknesses that ultimately derive from the minimalistic, "Ockham's razor" nature of the 2-step mechanism.[29] Also available elsewhere for the interested reader are 9 previously unavailable, mechanistic/physical insights that result from the 2-step mechanism,[4,29] insights which are expected to transfer to the synthesis of supported nanoparticle catalysts in contact with solution.[3−5]

CONCLUSIONS

In summary, the observed results (i) provide the first-available kinetic evidence that nucleation from at least the prototype supported Ir(1,5-COD)Cl/γ-Al_2O_3 precatalyst in contact with acetone is bimolecular. Combined with our prior results,[5] the kinetic data are consistent with and strongly supportive of a mechanism containing four main steps: K_{Diss} equilibrium between Ir(1,5-COD)Cl/γ-Al_2O_3 and Ir(1,5-COD)Cl(solvent), Ir(1,5-COD)Cl(solvent) solution-based *bimolecular* nucleation, fast nanoparticle capture via γ-Al_2O_3 and subsequent nanoparticle growth between $Ir(0)_n/\gamma$-Al_2O_3 and Ir(1,5-COD)Cl(solvent). Our results also (ii) disprove the solution-based unimolecular, as well as hypothetical, net termolecular nucleation mechanism. In combination with our prior studies[5] (studies that ruled out the all "solid-oxide-based" and all "solution-based" nucleation and growth pathways) a total of four mechanisms have been disproven to date en route to the proposed mechanism for the Ir(1,5-COD)Cl/γ-Al_2O_3 to $Ir(0)_{\sim 900}/\gamma$-Al_2O_3 supported-nanoparticle formation system in contact with solution shown back in Scheme 2, but hereby modified by bimolecular nucleation, Scheme 4.

In addition, the present results also (iii) promise to continue[3−5,20] to help drive the syntheses of the next generation of composition, size, and shape controlled supported-nanoparticle catalysts. Specifically, (iv) the present results reveal that the previous k_{1obs} used in the first-available mechanism-based equation for nanoparticle size control[30] should be replaced by $2k_{1obs(bimol)}[A]^1$ (i.e., and since $2k_{1obs(bimol)}[A]^2 = k_{1obs}[A]^1$ as demonstrated by the results herein). That said, it is (v) noteworthy that the treatment of nucleation as a *pseudo-first order* process remains a convenient way to analyze nucleation kinetic data since the relationship $2k_{1(bimol)}[A]^2 = k_{1obs}[A]$ holds during the induction period where [A] is effectively constant to a high approximation. Finally and most significantly, the results presented herein (vi) support a growing literature where simple, bimolecular nucleation appears to be common, for example also in protein aggregation[31] or aerosol formation.[32] The evidence herein and elsewhere[31,32] for nucleation being kinetically bimolecular is of considerable significance since it begins to establish *a just now emerging picture of bimolecular nucleation across broader parts of nature*.[31,32] That picture of bimolecular nucleation being closer to the "rule", rather than the exception, *for strongly bonding systems*, thereby and therefore also (vii) provides growing experimental evidence that disproves at least parts of classical

dx.doi.org/10.1021/cs2006422 | ACS Catal. 2012, 2, 298−305

nucleation theory and its higher molecularity, M_n critical nucleus concept,[18,33,34] again at least in strongly bonded (e.g., Ir and, by implication, other metal−metal), *irreversibly associating* systems (i.e., and as opposed to latexes[35] or other,[36] *weakly intermolecularly, reversibly associated systems*). Our results argue for the replacement of the "critical nucleus" concept of nucleation theory by a *kinetically effective nucleus* concept for strong binding systems. Note here the difference between the *kinetically effective nucleus* and the *catalytically effective nucleus* (the latter for cyclohexene hydrogenation) as defined elsewhere.[30] Given the significance and broad applicability of nucleation and growth phenomenon across nature, the present evidence in support of bimolecular nucleation for supported transition-metal nanoparticle catalyst formation is, therefore, both fundamental and important.

■ ASSOCIATED CONTENT

Supporting Information

Derivation of (i) the proposed bimolecular, Ir(1,5-COD)Cl-(solvent) solution-based, mechanism; (ii) the integrated rate equation for the two-step bimolecular nucleation and autocatalytic surface-growth mechanism; (iii) the proposed bimolecular, solution-based, mechanism for the mixed cyclohexane/acetone solvent system; (iv) the hypothetical, solution-based, termolecular nucleation mechanism; (v) the hypothetical, solution-based, termolecular nucleation mechanism for the mixed cyclohexane/acetone solvent system; (vi) the unconstrained and constrained fits of the termolecular nucleation mechanism to the $k_{1obs(bimol)}$ vs $[\gamma\text{-}Al_2O_3]_{sus}$ and [acetone] data; and (vii) fits of the k_{1obs} vs $[\gamma\text{-}Al_2O_3]_{sus}$ and [acetone] data to the bimolecular nucleation mechanism. This material is available free of charge via the Internet at http://pubs.acs.org.

■ AUTHOR INFORMATION

Corresponding Author

*E-mail: rfinke@lamar.colostate.edu.

Funding

We gratefully acknowledge support from the Chemical Sciences, Geosciences, and Biosciences Division, Office of Basic Energy Sciences, Office of Science, U.S. Department of Energy, Grant DE-FG02-03ER15688.

■ REFERENCES

(1) Schlögl, R.; Hamid, S. B. A. *Angew. Chem., Int. Ed.* **2004**, *43*, 1628−1637.

(2) Bell, A. T. *Science* **2003**, *299*, 1688−1691.

(3) Mondloch, J. E.; Bayram, E.; Finke, R. G. *J. Mol. Catal. A: Chem.* **2011**, in press, DOI:10.1016/j.molcata.2011.11.011.

(4) Mondloch, J. E.; Wang, Q.; Frenkel, A. I.; Finke, R. G. *J. Am. Chem. Soc.* **2010**, *132*, 9701−9714.

(5) Mondloch, J. E.; Finke, R. G. *J. Am. Chem. Soc.* **2011**, *133*, 7744−7756.

(6) The eight prototype criteria previously developed[4] are (i) a compositionally and structurally well-defined supported precatalyst (accomplished previously via inductively coupled plasma optical emission spectroscopy, CO/IR trapping experiments as well as XAFS spectroscopy[4]); (ii) a system in contact with solution and formed under low temperature conditions; and (iii) a system where a balanced stoichiometry of the supported-nanoparticle formation reaction is established (e.g., Scheme 1, as previously confirmed elsewhere[4]), leading to a well defined $Ir(0)_{\sim 900}/\gamma\text{-}Al_2O_3$ supported-nanoparticle heterogeneous catalyst (confirmed for the present system by TEM and XAFS[4]). In addition, a prototype system should (iv) yield an active and long-lived catalyst, and hence (v) provide a system where the initial kinetic and mechanistic studies of the in situ catalyst formation are worth the effort. The prototype system should also (vi) yield reproducible and quantitative kinetic data so that quantitative conclusions and mechanistic insights can be drawn;[5] and ideally will also (vii) allow a comparison to a kinetically and mechanistically well-studied nanoparticle formation system in solution for any insights that comparison might allow.[5] Lastly, once that prototype system is in hand, one would also like to be able to (viii) systematically vary key synthetic variables such as the support, solvent and metal precursor to reveal their effects on supported-nanoparticle formation in contact with solution.

(7) Watzky, M. A.; Finke, R. G. *J. Am. Chem. Soc.* **1997**, *119*, 10382−10400.

(8) The details on the typically observed range in k_1 values of $\sim 10^{1.2}$ h^{-1} were derived over a >7 year period from data obtained from multiple investigations and by multiple investigators for the well studied $P_2W_{15}Nb_3O_{62}^{9-}$ polyoxoanion-stabilized $Ir(0)_{\sim 300}$ nanoparticle formation system, and were originally described in: Widegren, J. A.; Bennett, M. A.; Finke, R. G. *J. Am. Chem. Soc.* **2003**, *125*, 10301−10310 (specifically p. 10304).

(9) (a) Besson, C.; Finney, E. E.; Finke, R. G. *J. Am. Chem. Soc.* **2005**, *127*, 8179−8184. (b) Besson, C.; Finney, E. E.; Finke, R. G. *Chem. Mater.* **2005**, *17*, 4925−4938. (c) Finney, E. E.; Finke, R. G. *Chem. Mater.* **2008**, *20*, 1956−1970.

(10) The rate and equilibrium constants in eq 2 are designated k_1'' and K_{Diss}' because the dimer $[Ir(1,5\text{-}COD)Cl]_2$ is present in solution, rather than the Ir(1,5-COD)Cl(solvent) monomer.[5] The presence of the $[Ir(1,5\text{-}COD)Cl]_2$ dimer is due to a change in the reaction conditions; a mixed solvent system of cyclohexane plus acetone was used to probe the acetone dependence, while just acetone was used to probe the $\gamma\text{-}Al_2O_3$ dependence.

(11) Laxson, W.; Ott, L. S.; Finke, R. G. Unpublished results and experiments in progress.

(12) Li, F.; Gates, B. C. *J. Phys. Chem. B* **2004**, *108*, 11259−11264.

(13) Colombi Ciacchi, L.; Pompe, W.; De Vita, A. *J. Am. Chem. Soc.* **2001**, *123*, 7371−7380.

(14) Henglein, A.; Giersig, M. *J. Phys. Chem. B* **1999**, *103*, 9533−9539.

(15) Angermund, K.; Bühl, M.; Endruschat, U.; Mauschick, F. T.; Mörtel, R.; Mynott, R.; Tesche, B.; Waldöfner, N.; Bönnemann, H.; Köhl, G.; Modrow, H.; Hormes, J.; Dinjus, E.; Gassner, F.; Haubold, H.-G.; Vad, T.; Kaupp, M. *J. Phys. Chem. B* **2003**, *107*, 7507−7515.

(16) Yao, T.; Sun, Z.; Li, Y.; Pan, Z.; Wei, H.; Nomura, M.; Niwa, Y.; Yan, W.; Wu, Z.; Jiang, Y.; Liu, Q.; Wei, S. *J. Am. Chem. Soc.* **2010**, *132*, 7696−7701.

(17) Finney, E. E.; Finke, R. G. *J. Colloid Interface Sci.* **2008**, *317*, 351−374.

(18) (a) Agreement between theory and experiment within nucleation theory to a few orders of magnitude is often considered a great success,[33] while disagreements between theoretical predictions and experimental results as large as 10^6 to 10^{10} are known.[34] (b) See also the following reference for a detailed list, and compelling discussion, of the multiple assumptions and resultant failures of classical nucleation theory (CNT): Erdemir, D.; Lee, A. Y.; Myerson, A. S. *Acc. Chem. Res.* **2009**, *42*, 621−629.

(19) Lamer, V. K.; Dinegar, R. H. *J. Am. Chem. Soc.* **1950**, *72*, 4847−4854.

(20) Mondloch, J. E.; Yan, X.; Finke, R. G. *J. Am. Chem. Soc.* **2009**, *131*, 6389−6396.

(21) Hornstein, B. J.; Finke, R. G. *Chem. Mater.* **2004**, *16*, 139−150.

(22) Lin, Y.; Finke, R. G. *Inorg. Chem.* **1994**, *33*, 4891−4910.

(23) Motulsky, H.; Christopoulos, A. *Fitting Models to Biological Data Using Linear and Nonlinear Regression*; Oxford University Press: New York, 2004.

(24) More specifically the hypothetical "concentrations" of suspended $\gamma\text{-}Al_2O_3$ binding sites for "Ir(1,5-COD)Cl" are treated as if they increase linearly when in contact with solution (or, really and

physically, as if they increased linearly with the amount of solvent-exposed γ-Al_2O_3 surface area).

(25) To quantitatively compare R^2 values, the fit of the unimolecular mechanism to the k_{1obs} vs $[\gamma\text{-}Al_2O_3]_{sus}$ data and the bimolecular mechanism to the $k_{1obs(bimol)}$ vs $[\gamma\text{-}Al_2O_3]_{sus}$ data, the K_{Diss} equilibrium was constrained to its previously determined value[5] of 0.013 in the bimolecular fit. This is necessary because the correlation coefficient (i.e., R^2) will increase when more parameters are allowed to vary within the fit;[23] one parameter (i.e., k_1') varies in the unimolecular case,[5] while two parameters (i.e., $k_{1(bimol)}'$ and K_{Diss}) vary in the bimolecular case.

(26) (a) Outlier analysis of the $k_{1obs(bimol)}$ vs acetone data to the bimolecular mechanism (eq 10) suggested that the data point of 1.85 $\times$ 10^{-3} h^{-1} M^{-1}, 0.91 M be excluded from the "fit". This was confirmed via the *t*-test[26b] at the 95% confidence level. In short, this means that one less point (a total of 24 data points) is present in the $k_{1obs(bimol)}$ vs [acetone] plot, than the original k_{1obs} vs [acetone] plot.[5] (b) Harris, D. C. *Quantitative Chemical Analysis*, 6th ed.; W.H. Freeman Company: New York, 2003.

(27) To ensure that the removal of the data point at 1.85 $\times$ 10^{-3} h^{-1} M^{-1}, 0.91 M did not significantly change the resultant R^2 value in the $k_{1obs(bimol)}$ vs [acetone] fit, it was also removed (also statistically justified via the *t* test[26b]) from the k_{1obs} vs [acetone] fit. The R^2 value changes slightly from 0.245 to 0.248. Hence, removal of the outlying datum point is not an issue in the resultant interpretation of the data.

(28) Note here that we do not mean to imply the possibility of an actual, statistically improbable, *concerted* 3-body termolecular collision in solution. True termolecular reactions tend to be gas phase reaction where the third body is needed to remove excess heat from the reaction products, see: Moore, J. W.; Pearson, R. G. *Kinetics and Mechanism*, 3rd ed.; Wiley: New York, 1981; see p.226, Table 6.8. Instead, any hypothetical mechanism α $[A]^3$ would presumably come from at least one prior, bimolecular equilibrium step and an associated K_{eq}. The hypothetical net termolecular reaction is treated as a pseudo-elementary step[7] in the derivation provided in the Supporting Information.

(29) Finney, E. E.; Finke, R. G. *Chem. Mater.* **2009**, *21*, 4692−4705 ; see p4702.

(30) Watzky, M. A.; Finney, E. E.; Finke, R. G. *J. Am. Chem. Soc.* **2008**, *130*, 11959−11969.

(31) Knowles, T. P. J.; Waudby, C. A.; Devlin, G. L.; Cohen, S. I. A.; Aguzzi, A.; Vendruscolo, M.; Terentjev, E. M.; Welland, M. E.; Dobson, C. M. *Science* **2009**, *326*, 1533−1537.

(32) Sipilä, M.; Berndt, T.; Petäjä, T.; Brus, D.; Vanhanen, J.; Stratmann, F.; Patokoski, J.; Mauldin, R. L. III; Hyvärinen, A.-P.; Lihavainen, H.; Kulmala, M. *Science* **2010**, *327*, 1243−1246.

(33) Oxtoby, D. W. *Acc. Chem. Res.* **1998**, *31*, 91−97.

(34) Dixit, N. M.; Zukoski, C. F. *Phys. Rev. E* **2002**, *66*, 051602.

(35) (a) Wette, P.; Schöpe, H. J.; Palberg, T. *J. Chem. Phys.* **2005**, *123*, 174902. (b) Zhang, T. H.; Liu, X. Y. *Angew. Chem., Int. Ed.* **2009**, *48*, 1−6.

(36) Rusyniak, M.; Abdelsayed, V.; Campbell, J.; Samy El-Shall, M. *J. Phys. Chem. B* **2001**, *105*, 11866−11872.